Expert Systems with Applications 40 (2013) 471–479

Contents lists available at SciVerse ScienceDirect

Expert Systems with Applications

journal homepage: www.elsevier.com/locate/eswa

An innovative blemish detection system for curved LED lenses

Yuan-ShyiPeter Chiu, Hong-Dar Lin *

Department of Industrial Engineering and Management, Chaoyang University of Technology, 168 Jifong E. Rd., Wufong District, Taichung 41349, Taiwan

ARTICLE INFO

Keywords:
Blemish detection system
Curved LED lens
Discrete cosine transform
Energy features
Grey clustering

ABSTRACT

The functions of LED lenses include focusing, beauty, and protection to avoid the waste of light and light pollution. Nevertheless, LED lens with a transparent and curved surface is more difficult to detect the visual blemishes than electronic and optical components by current computer vision systems. This research proposes an innovative blemish detection system to detect visual blemishes of the curved LED lenses. A spatial domain image with equal sized blocks is converted to discrete cosine transform (DCT) domain and some representative energy features of each DCT block are extracted. These energy features of each block are integrated by the Hotelling's T-squared statistic and the suspected blemish blocks can be determined by the multivariate statistical method. Then, the grey clustering technique based on the block grey relational grades is applied to further confirm the block locations of real blemishes. Finally, a simple thresholding method is applied to set a threshold for distinguishing between defective areas and uniform regions. Experimental results show that the proposed system achieves a high 95.46% probability of correctly discriminating visual blemishes from normal regions and a low 0.13% probability of erroneously detecting normal regions as blemishes on curved surfaces of LED lenses.

1. Introduction

A lens is an optical device with perfect or approximate axial symmetry which transmits and refracts light, converging or diverging the beam. Lenses are typically made of glass or transparent plastic. Optical lenses are transparent components made from optical-quality materials and curved to converge or diverge transmitted rays from an object. These rays then form a real or virtual image of the object. There are many types of optical lenses. Optical lenses are widely used in cell phones, notebooks, automotive lights, digital cameras, scanners, head lamps etc.

A light-emitting diode (LED) is a semiconductor device that emits visible light when an electric current passes through the semiconductor chip. Compared with incandescent and fluorescent illuminating devices, LEDs have lower power requirement, higher efficiency, and longer lifetime. Typical applications of LED components include indicator lights, LCD panel backlighting, fiber optic data transmission, etc. To meet consumer and industry needs, LED products are being made in smaller sizes, which increase difficulties of product inspection. The functions of LED lenses include focusing, beauty, and protection to avoid the waste of light and light pollution. An LED without the assistance of lens focus function cannot project light to the intended location. Therefore, LED lenses are invented to improve the light scattering problems of LEDs and they are widely applied to hand flashlights and traffic lights applications. Fig. 1 shows the common LED lens and LED lens product.

Lens inspection requires special physical conditions, particularly in terms of lighting. In the real working situation, each inspected lens is brought into the inspector's field of vision. The lenses are round and transparent; the blemish to be inspected could be located on the external surface of the lenses or inside. A lens presents a certain thickness and a certain curvature, both of which vary. At times, lenses provide the same perceptive result as a magnifying glass, and the blemishes are all the more difficult to track down and to locate in the area of the lens. The majority of blemishes are not only very small but also they are extremely diverse and can assume various forms. Fig. 2 presents LED lenses with and without visual blemishes.

Currently, the most common detection methods for LED lens blemishes are human visual inspection. Human visual inspection is tedious, time-consuming and highly dependent on the inspectors' experiences, conditions, or moods. Erroneous judgments are easily made because of inspectors' subjectivity and eye fatigues. Difficulties exist in precisely inspecting tiny flaws by machine vision systems because when product images are being captured, the area of a tiny flaw could expand, shrink or even disappear due to uneven illumination of the environment, transparent and curved surfaces of the product, and so on. Seeing the great need for an automated visual detection scheme for LED lens blemishes, we propose an innovative detection system applying block discrete cosine transform (BDCT) and gray clustering technique to overcome the difficulties of traditional machine vision systems.

* Corresponding author. Tel.: +886 4 2332 3000x4258; fax: +886 4 2374 2327.
E-mail address: hdlin@cyut.edu.tw (H.-D. Lin).

0957-4174/$ - see front matter © 2012 Elsevier Ltd. All rights reserved.
http://dx.doi.org/10.1016/j.eswa.2012.07.041

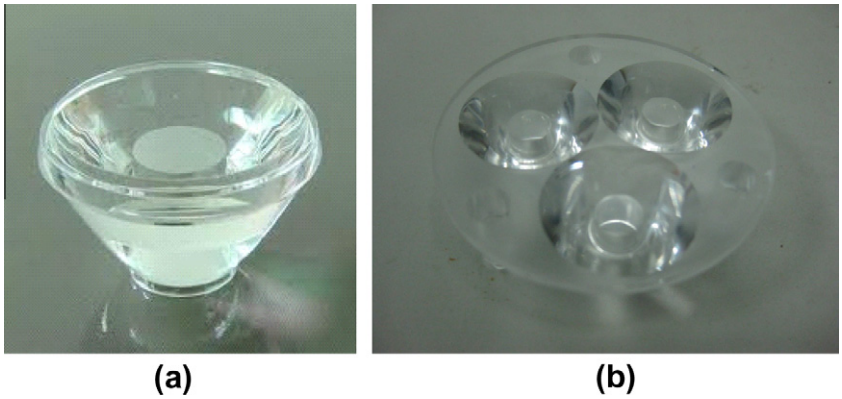

Fig. 1. (a) An LED lens (side view); (b) an LED lens product (top view).

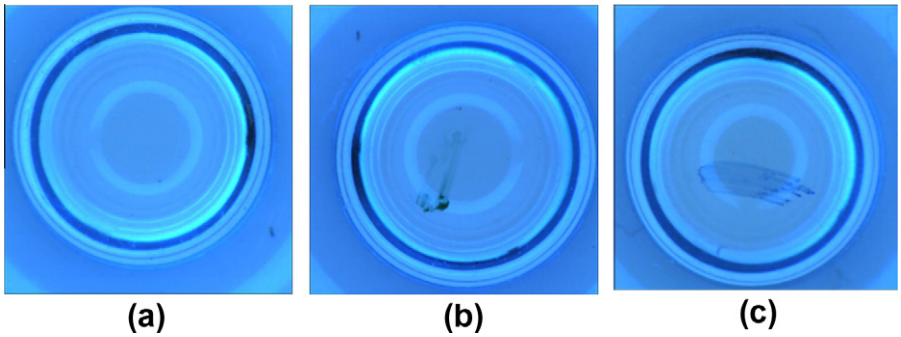

Fig. 2. LED lenses with and without visual blemishes (from top view) (a) LED lens without blemish; (b) LED lens with dirt blemishes; (c) LED lens with scratch blemishes.

2. Blemish inspection methods

Inspection of surface blemishes has become a critical task for manufacturers who strive to improve product quality and production efficiency (Lin & Lin, 2009; Lin, Lin, Chung, & Lin, 2008). Blemish detection techniques, generally classified into the spatial domain and the frequency domain, compute a set of textural features in a sliding window and search for significant local deviations among the feature values. Latif-Amet, Ertüzün, and Ercil (2000) presented wavelet theory and co-occurrence matrices for detection of blemishes encountered in textile images and classify each subwindow as defective or non-defective with a Mahalanobis distance. Cho, Chung, and Park (2005) applied the adaptive threshold technique and morphology method to detect defects from images of uniform fabrics for developing a real-time vision system.

As to techniques in the frequency domain, Chan and Pang (2000) used the Fourier transform to detect fabric defects. Tsai and Hsiao (2001) proposed a wavelet transform based approach for inspecting local defects embedded in homogeneous textured surfaces. By properly selecting the smooth sub-image or the combination of detail sub-images in different decomposition levels for backward wavelet transform, regular, repetitive texture patterns can be removed and only local anomalies are enhanced in the reconstructed image. Also, Lin and Ho (2007) developed a novel approach that applies discrete cosine transform based enhancement for the detection of pinhole defects on passive component chips.

As to inspecting blemishes of lenses, Rebsamen, Boucheix, and Fayol (2010) described quality control tasks in the optical industry from a work analysis of optical lens inspection to a training program. Martínez, Ortega, García, and García (2009) developed a vision sensor planning system for automated inspection of headlamp lenses. This system uses the lens CAD, a vision sensor model and the customer requirements describing by a fuzzy approach, to achieve an optimal set of viewpoints by genetic algorithm. Bazin, Cole, Kett, and Nixon (2006) proposed a novel method for the industrial inspection of ophthalmic contact lenses in a time constrained production line environment. Perng, Wang, and Chen (2010) presented a new inspection system that uses machine vision to detect optical blemishes in quasi-contact lenses. The optical region of the lens image is first segmented, then the middle axes of each fringe on the optical region are determined. Three features of the fringe are extracted to create a mapping of the original features to a semantic description of the textures. Finally, the quality of the quasi-contact lens is determined by a control chart procedure. Therefore, most of the existing researches focus on inspections of optical lenses, headlamp lenses, and contact lenses. They do not detect blemishes with the properties of tiny blemishes on LED lenses. Consequently, we present a new approach using block discrete cosine transform and grey clustering for blemish detection of the transparent and curved LED lens surfaces.

Ahmed, Natarajan, and Rao (1974) first defined DCT as one-dimensional (1-D) and suitable for 1-D digital signal processing. Most of the researchers that apply DCT for image processing focused on image compression and image reconstruction, because DCT has the property of packing the most information into the fewest coefficients (Gonzalez & Woods, 2008). However, due to the lack of an efficient algorithm, DCT had not been applied as widely as its properties imply. Only until recently, many algorithms and VLSI architectures for the fast computation of DCT have been proposed (Kok, 1997). To enhance edges of remote sensing image data in the DCT domain, Chen, Latifi, and Kanai (1999) developed new and fast algorithms that involve three steps: high-pass filtering, gray levels adding, and contrast stretching.

Grey system proposed by Deng (1989) means that the information within a system is partially unknown. Grey theory provides the applications of clustering analysis, relational analysis, predication, and decision for the grey system. The grey theory has the advantage of being able to deal with complex problems involving uncertain or incomplete systems. Grey clustering is a common grey theory application, which classifies unknown samples into specified groups by comprehensively integrating the various attribute intensities of each sample (Tsai, Hsiao, & Hung, 2006). Heng (2010) analyzed infrared images based on grey system and applied grey clustering to filter out possible objects for detecting infrared targets. Huang (2008) employed image processing techniques and a modified unsupervised grey clustering algorithm to estimate the location of each die and identify the spot number accurately and effectively. Lin, Wu, and Huang (2009) proposed a method for incipient fault diagnosis in oil-immersed transformers using grey clustering analysis. Their method could avoid the determination of the linguistic variables, membership functions, inference rules, network architecture, and parameters assignment, and is easy to implement in the portable device.

Hu, Chen, Hsu, and Tzeng (2002) proposed a grey clustering method incorporating the grey relational grades into learning rules of self-organizing feature maps for solving classification and traveling salesman problems. Lin and Lee (2009) developed an improved model integrating grey number into grey clustering technique to deal with the evaluation problems under the condition of insufficient and uncertain information. Tsai et al. (2006) used grey clustering operation for color image evaluation in product form and color design. Madhuri and Chandulal (2010) combined grey relational analysis and grey clustering to evaluate the website for providing useful information for users and estimating the validation and popularity of the websites. Therefore, grey clustering technique has been successfully applied in the fields of engineering detection, classification, decision-making, product design, performance evaluation, etc. in recent years.

3. Proposed system

By regarding an input image as a matrix, we can perform the DCT transformation to transform a spatial domain image into the frequency domain. A spatial domain image with equal sized blocks is converted to DCT domain and some representative energy features of each DCT block are extracted. These energy features of each block are integrated by the T-squared statistic and the suspected blemish blocks can be determined by the multivariate statistical method. Then, the grey clustering algorithm based on block grey relational grades is conducted to further confirm the block locations of real blemishes. Finally, a simple segmentation method is applied to set a threshold for distinguishing between defective areas and uniform regions. Therefore, the visual blemishes on the curved surfaces of LED lenses can be accurately detected and located by the proposed method. Fig. 3 shows the concept diagram of the proposed method.

3.1. Image preprocessing

In most computer vision systems, the region of interest (ROI) is a rectangle (block) that contains the object to be investigated. The use of ROI can avoid the interference of uninterested regions when mask (template) computations or frequency transformations are conducted. If an image containing uninterested regions is transformed into the BDCT domain, the uninterested region (e.g. background) can significantly interfere in the frequency analysis of the ROI. Therefore, after we use CCD and XY electronic control table to acquire the image of the target LED lens, we produce a target mask to delineate the ROI, the region of the target LED lens. Then we obtain a mixed image by combining the target region with a manipulated background to decrease the interference of an uninterested region (the original background). This mixed image will then be used as the input for further BDCT transformation.

When capturing the images of our testing samples, we set the LED lenses on a carrier plate which is attached to an XY electronic control table and which moves while the camera stays fixed. As the carrier plate moves to have the image of the next LED lens captured, the movement of the carrier plate might cause the CCD to deviate from its original position and the image capturing device to vibrate. Thus, the images of all the LED lenses might be captured with slight differences; that is, not all LED lenses are located in the exactly same positions in their individual images. As a result, a target mask is needed for each image to specify the location of the target LED lens. Fig. 4 presents the procedure for producing a target mask for a target LED lens.

In Fig. 4(a), the testing image is first captured and input. Second, a preliminary edge detection is conducted on the image to roughly indicate the boundary of the target region by using Sobel operators Gonzalez & Woods, 2008 . In Fig. 4(b), the white regions mean the boundaries of the target LED lens. Based on the boundary information, the mass center and radius of the target region can be determined to specify the exact region of the target. For each testing image, there is a corresponding target mask to delineate the exact region of the target LED lens (ROI). Fig. 4(c) shows the mass center and radius of the target region and Fig. 4(d) is the result of producing target mask image. After the target mask image is produced, we can specify the accurate region of the target LED.

After the target mask is built, the target LED lens is delineated in a circular shape. Since BDCT transformation can process images of rectangular shapes, a specially-made background must be added to convert the circular target region into a rectangular one. A mixed image is thus produced by integrating the circular target region into a background that is formed by duplicating the average gray level of the target region. With such a manipulated background, we not only obtain a rectangular region for BDCT transformation but also minimize the affect of the non-target region. Once the mixed image is transformed into the BDCT domain, the non-target region will not interfere in the frequency analysis of the target region. Therefore, better results of image enhancement can be obtained by adding the manipulated background. Fig. 4(e) shows the mixed image.

3.2. Block discrete cosine transform

The inspection task of this paper involves detecting novel but obscurely faulty items, visual blemishes on LED lenses of optical components. Many of these unanticipated blemishes are extremely small in size and cannot be described by explicit measures, thus making automated blemish detection difficult. Since DCT has the advantages of packing the most information into the fewest coefficients and minimizing reconstruction errors, only a small amount of information of a detailed image will be lost during the image processing procedures (Gonzalez & Woods, 2008). Such advantages make DCT suitable and favorable for our study of visual blemish detection of optical components. To increase the computational efficiency of DCT, the BDCT is adopted that we divide an image into non-overlapping image blocks of equal size which can be conducted DCT individually instead of taking one transform on an entire image.

Eq. (1) gives the expression for computing the BDCT of a digital image $d_{x,y}$ of block size $P \times Q$. This expression must be computed for all values of $u = 0, 1, 2, \ldots, P-1$, and also for all values of $v = 0, 1, 2, \ldots, Q-1$. While u and v are frequency variables, x and y are spatial variables.

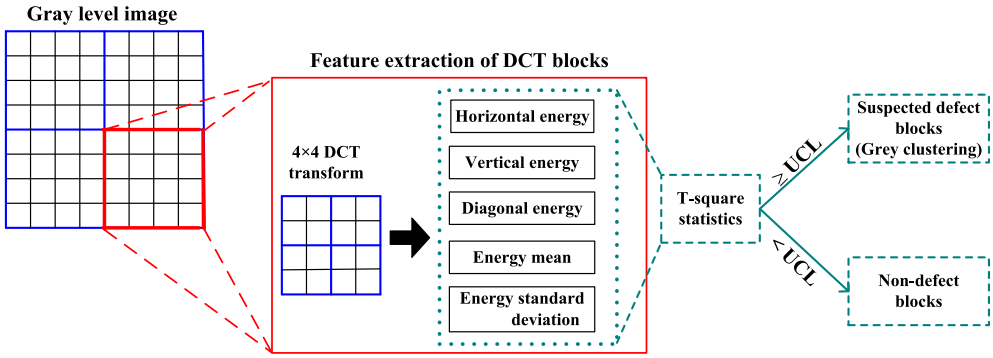

Fig. 3. Concept diagram of the proposed methods.

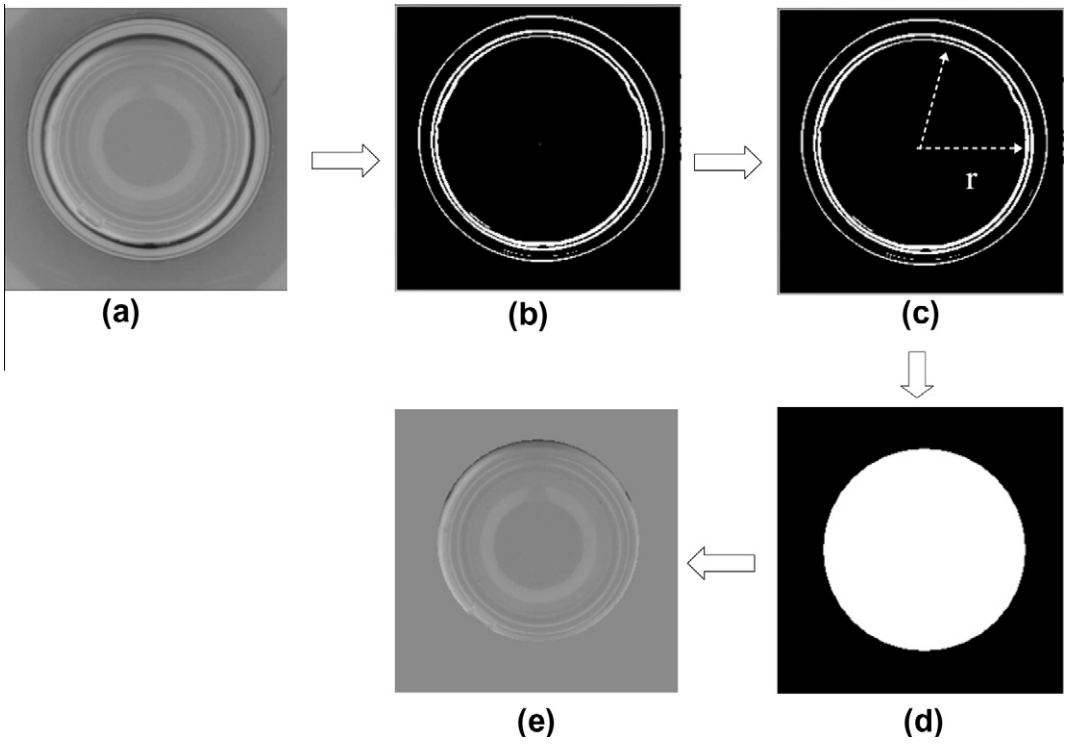

Fig. 4. Preprocessing procedures of the proposed method (a) the original testing image; (b) the edge detection result by the Sobel operators; (c) the mass center and radius of the target region; (d) the result of producing target mask image; (e) the mixed image.

$$D_{u,v} = \rho(u)\rho(v)\sum_{x=0}^{P-1}\sum_{y=0}^{Q-1} d_{x,y}\cos\left[\frac{(2x+1)u\pi}{2P}\right]\cos\left[\frac{(2y+1)v\pi}{2Q}\right], \quad (1)$$

where

$$\rho(u) = \begin{cases} \sqrt{\frac{1}{P}}, & u = 0 \\ \sqrt{\frac{2}{P}}, & u = 1,2,3,\ldots,P-1 \end{cases},$$

$$\rho(v) = \begin{cases} \sqrt{\frac{1}{Q}}, & v = 0 \\ \sqrt{\frac{2}{Q}}, & v = 1,2,3,\ldots,Q-1 \end{cases}, \quad \begin{cases} u = 0,1,2,3,\ldots,P-1 \\ v = 0,1,2,3,\ldots,Q-1 \\ x = 0,1,2,3,\ldots,P-1 \\ y = 0,1,2,3,\ldots,Q-1 \end{cases}.$$

The power spectrum $P(u,v)$ of image $d_{x,y}$ is defined as:

$$P(u,v) = |D_{u,v}|^2. \quad (2)$$

That is, the sum of the squares of the DCT coefficients is the energy of the block.

As the origin of the BDCT coefficients has a very huge frequency component, it is sometimes called the Direct Current (DC) component of the BDCT frequency domain, while other coefficients are called the Alternating Current (AC) components. The DC coefficients in the upper left corner reflect information of lower frequencies, whereas the AC coefficients in the lower right corner reflect that of higher frequencies. BDCT has the property of concentrating the dominant energy of a typical image in the low-frequency components. This means that the coefficients of the high-frequency components are close to zero, and therefore negligible in most cases (Gonzalez & Woods, 2008).

The 2-D and 3-D BDCT spectrum diagrams of an LED lens image in Fig. 5(b) and (c) show that a lot of energy concentrates in the origin ($u = 0, v = 0$) and that the energy decreases gradually from the origin and the low frequency zone on the top-left side to the high frequency zone on the bottom-right side. In the BDCT domain, the tiny and low-contrast blemishes are not only significantly enhanced but also the gradually changing intensity levels of blemishes are removed.

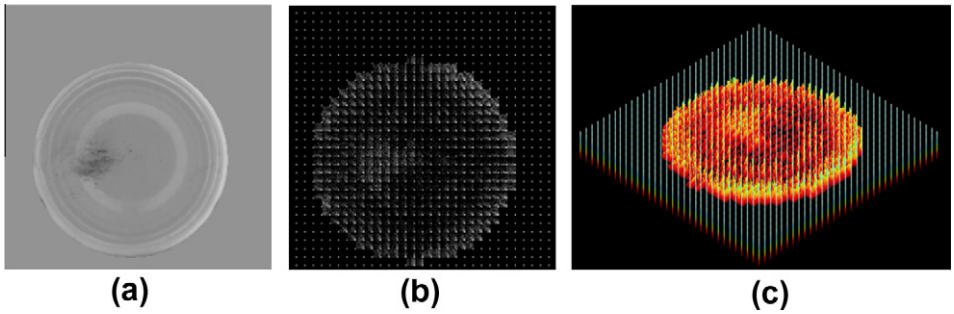

Fig. 5. Examples of the BDCT transformation (a) an LED lens image with visual blemishes; (b) the 2-D BDCT spectrum image; (c) the power spectra in 3-D perspective.

The edge pattern in a block can be fully captured from its DCT coefficients in frequency domain (Pan, 2002). The energy distribution in the DCT domain determines the edge patterns in the spatial block. One way of determining the features in the spatial block is by looking into the energy distribution in the 2D-DCT domain (Rao & Hwang, 1996). The energy concentrated in top horizontal region represents vertical edges in the block; the energy concentrated in left vertical region indicates horizontal edges in the block; and the energy concentrated in diagonal region implies diagonal edges in the block.

Five energy features of a BDCT are expressed as follows:

$$E_H = \left[\sum_{u=0}^{P-1}\sum_{v=0}^{Q-1}(v+1)^2 \times D_{u,v}^2\right]^{1/2} \quad u+v \neq 0, \tag{3}$$

$$E_V = \left[\sum_{u=0}^{P-1}\sum_{v=0}^{Q-1}(u+1)^2 \times D_{u,v}^2\right]^{1/2} \quad u+v \neq 0, \tag{4}$$

$$E_D = \left[\sum_{u=0}^{P-1}\sum_{v=0}^{Q-1}(u+1)\times(v+1) \times D_{u,v}^2\right]^{1/2} \quad u+v \neq 0, \tag{5}$$

$$E_M = \frac{1}{P\times Q}\sum_{u=0}^{P-1}\sum_{v=0}^{Q-1}D_{u,v}, \tag{6}$$

$$E_S = \frac{1}{(P\times Q)-1}\sum_{u=0}^{P-1}\sum_{v=0}^{Q-1}(D_{u,v}-E_M)^2, \tag{7}$$

where $P \times Q$ is the block size of BDCT, D is frequency components of BDCT, u and v are frequency coordinates of BDCT, E_H is the horizontal energy value of a BDCT, E_V is the vertical energy value of a BDCT, E_D is the diagonal energy value of a BDCT, E_M is the average energy value of a BDCT, and E_S is the standard deviation of energy values of a BDCT.

3.3. Multivariate T-squared statistic

The five energy features extracted from a BDCT will be treated as five quality characteristics for multivariate statistical analysis. Normal texture images can be used to estimate the parameters of standard texture characteristics. The sample mean matrix ($\bar{X}$) and the sample covariance matrix (S) describe the properties of and the relations between the image characteristics of normal and blemish images. The covariance is a measure of the relationship between two random variables. Since the five energy features do not follow a multivariate normal distribution, a logarithmic transformation ($\log_{10}$) is conducted to transform the multivariate data to be normally distributed. The probability plot can be used to determine whether sample data conform to normal distributions (Montgomery & Runger, 2007). Therefore, the sample covariance matrix (S) of a normal image can be expressed as:

$$S = \begin{bmatrix} S_{E_H}^2 & S_{E_HE_V} & S_{E_HE_D} & S_{E_HE_M} & S_{E_HE_S} \\ S_{E_HE_V} & S_{E_V}^2 & S_{E_VE_D} & S_{E_DE_M} & S_{E_VE_S} \\ S_{E_HE_D} & S_{E_VE_D} & S_{E_D}^2 & S_{E_DE_M} & S_{E_DE_S} \\ S_{E_HE_M} & S_{E_DE_M} & S_{E_DE_M} & S_{E_M}^2 & S_{E_ME_S} \\ S_{E_HE_S} & S_{E_VE_S} & S_{E_DE_S} & S_{E_ME_S} & S_{E_S}^2 \end{bmatrix}_{5\times5}, \tag{8}$$

where S_p^2 is the sample variance of the p characteristic of a normal image, S_{pq} is the sample covariance of the p and q characteristics of a normal image. The sample mean matrix ($\bar{X}$) of a normal image can be defined as:

$$\overline{X_i} = \begin{bmatrix} \overline{X_1} \\ \overline{X_2} \\ \overline{X_3} \\ \overline{X_4} \\ \overline{X_5} \end{bmatrix}_{5\times1} = \begin{bmatrix} \log_{10}\overline{E_H} \\ \log_{10}\overline{E_V} \\ \log_{10}\overline{E_D} \\ \log_{10}\overline{E_m} \\ \log_{10}\overline{E_s} \end{bmatrix}_{5\times1},$$

where $\overline{E_H}$: average of block horizontal energy values
$\overline{E_V}$: average of block vertical energy values
$\overline{E_D}$: average of block diagonal energy values
$\overline{E_M}$: average of block energy values
$\overline{E_S}$: standard deviation of block energy values

The T-squared statistic of a BDCT with five energy features of a testing image in the multivariate statistical model can be defined as (Montgomery, 2009):

$$T^2 = n(X_i - \overline{X_i})^T S^{-1}(X_i - \overline{X_i}) \quad i = 1,2,3,\ldots,5, \tag{10}$$

where n is the number of observations in a BDCT unit, X is the mean matrix of energy features in a BDCT unit of a testing image. The control limits of the T^2 statistic are as follows:

$$UCL = \frac{p(m-1)}{m-p}F_{\theta,p,m-p}; \quad LCL = 0, \tag{11}$$

where F is a tabulated value of the F distribution at the significance level of θ. Therefore, if a BDCT unit of a testing image has a higher T-squared value, it implies that the region contains blemishes in the testing image. On the contrary, a lower T-squared value signifies that no blemish exist in the corresponding region of the image.

3.4. Grey clustering

The BDCT blocks with high T-squared values greater than the UCL are considered as the suspected blemish blocks in a testing image. The grey clustering technique will be conducted to further confirm the block locations of real blemishes. The initial sequences of the suspected blemish blocks can be presented as:

$$V = \{x_1, x_2, x_3, \ldots, x_p\}, \tag{12}$$

$$v_i = (E_H, E_V, E_D, E_M, E_S), \tag{13}$$

where p is the number of the suspected blemish blocks detected by the T-squared statistic. The grey relational grade of the two sequences: reference sequence v_i $(i = 1, 2, 3, \ldots, p)$ and comparative sequence v_j $(j = 1, 2, 3, \ldots, p)$ is defined as follows:

$$\gamma(v_i, v_j) = \frac{1}{u}\sum_{k=1}^{u}\gamma(v_i(k), v_j(k)), \tag{14}$$

where u is the number of energy features, and

$$\gamma(v_i(k), v_j(k)) = \left(\frac{\Delta_{\max} - \Delta_{ij}(k)}{\Delta_{\max} - \Delta_{\min}}\right)^{\zeta}, \tag{15}$$

where ζ is called distinguished coefficient and is set as 1 in this research, and

$$\Delta_{ij} = \| v_i(k) - v_j(k) \| \tag{16}$$

$$\Delta_{\max} = \max_{\forall k} \| v_i(k) - v_j(k) \| \tag{17}$$

$$\Delta_{\min} = \min_{\forall k} \| v_i(k) - v_j(k) \| \tag{18}$$

The higher degree of relation means the comparative sequence is more similar to the reference sequence than the others. Using the grey relational measure to train the grey cluster among of the given data points, and clustering the data according to the grey relational grades. The updated sequence is calculated by the equation:

$$v_i^*(k) = \frac{\sum_{j=1}^{n} n_{ij} v_j(k)}{\sum_{j=1}^{n} n_{ij}}, \quad k = 1, 2, 3, \ldots, 5, \tag{19}$$

$$\text{where,} \quad n_{ij} = \begin{cases} 1 & \text{if } \gamma_{ij} \geqslant \omega, \\ 0 & \text{if } \gamma_{ij} < \omega, \end{cases} \tag{20}$$

ω is a selected threshold with $0 < \omega < 1$. If all the updated sequences do not change (less than an allowance ε), the stop criterion of the iterations is:

$$|V_i - V_{i-1}| \leqslant \varepsilon \tag{21}$$

Finally, the convergent vector is viewed as the cluster center. The grey relational grades of the suspected blemish blocks are calculated to further identify the block locations of real blemishes. Fig. 6 demonstrates the changes of suspected blemish blocks found by grey clustering process in three different iterations.

Fig. 7 shows the results and differences performed the proposed method for detecting visual blemishes in LED lens. Fig. 7(b) presents the BDCT domain image of Fig. 7(a). Fig. 7(c) is the preliminary detected image with suspected blemish blocks (in white) when the energy features are integrated by the T-squared statistic. Fig. 7(d) depicts the primary detected image with blemish blocks re-confirmed by the grey clustering technique. Fig. 7(e) is a mixed image containing the detected blemish blocks and a manipulated background for locating blemish regions. Fig. 7(f) is the resulting binary images that display the flaws in black by the proposed blemish detection method. The results reveal that the visual flaws in LED lens are correctly segmented in the binary image, regardless of LED lens with transparent and curved surface.

4. Implementation and analyses

In this section, we implement the proposed approach and conduct experiments to evaluate its performance in detecting visual blemishes of LED lenses. To strengthen the visibility of the visual blemishes, we make use of the following equipments: a yellow ring lighting device, a USB 2.0 color CCD of ARTRAY company, a lens with 1 to 10 amplifications of changeable focal lengths, and a XYZ electronic control table with a controller. Experiments are conducted on 218 real LED lenses (including 148 normal lenses and 70 defective lenses) provided by a local manufacturing company of high quality LED lenses in Taiwan to evaluate the performance of the proposed approach. Fig. 8 demonstrates the configurations of the environment in which we scan real LED lenses to be used as testing samples in the experiments. Each image of the LED lens has a size of 256×256 pixels and a gray level of 8 bits. The visual blemish detection algorithm is edited in C language and executed on the 6th version of the C++ Builder complier on a personal computer (Pentium-4 2.8 GHz and 512 MB DDRII 667 Hz-RAM).

In industrial practice, when a detected blemish is larger than a pre-defined size, the inspection system alerts for the appearance of blemish. Sometimes, this information is not enough for quality control purpose because product quality measures not only the blemish volumes but also the blemish severity levels. The ranges of blemish sizes imply different severity levels of product blemishes. Thus, an inspection system should alert for the presence of blemishes, detect the blemish locations and calculate the blemish sizes in some applications. To verify the performance of the proposed method and traditional techniques, we compare the results of our experiments against those provided by professional inspectors by precisely matching the corresponding blemish locations and blemish sizes.

The performance evaluation indices, $(1 - \alpha)$ and $(1 - \beta)$, are used to represent correct detection judgments; the higher the two indices, the more accurate the detection results. Statistical

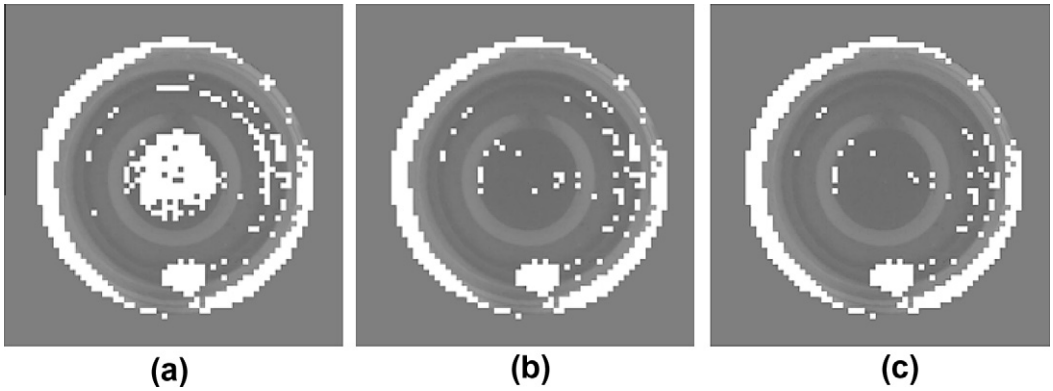

Fig. 6. The suspected blemish blocks found by grey clustering process in different iterations: (a) 0 iteration; (b) 3 iterations; (c) 5 iterations.

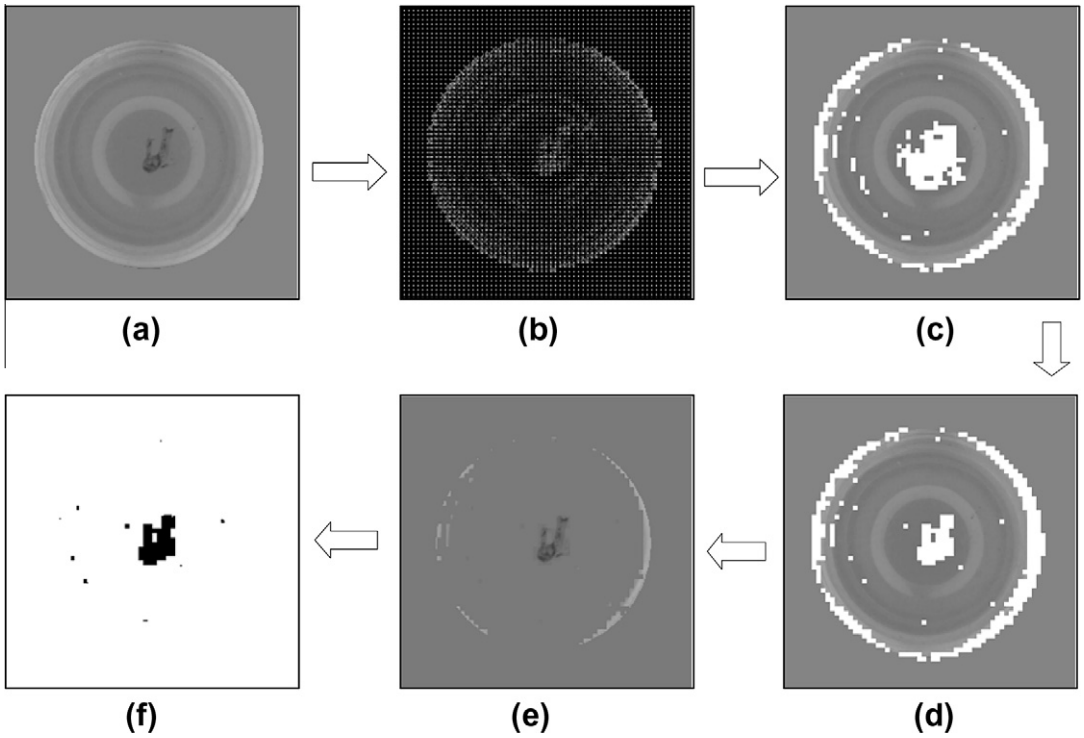

Fig. 7. The proposed procedure of detecting visual blemishes on LED lens (a) a testing image; (b) the BDCT domain image; (c) the suspected blemish blocks (in white) detected by T-squared statistic; (d) the re-confirmed blemish blocks by grey clustering; (e) the blemish blocks with a manipulated background; (f) resulting detected image.

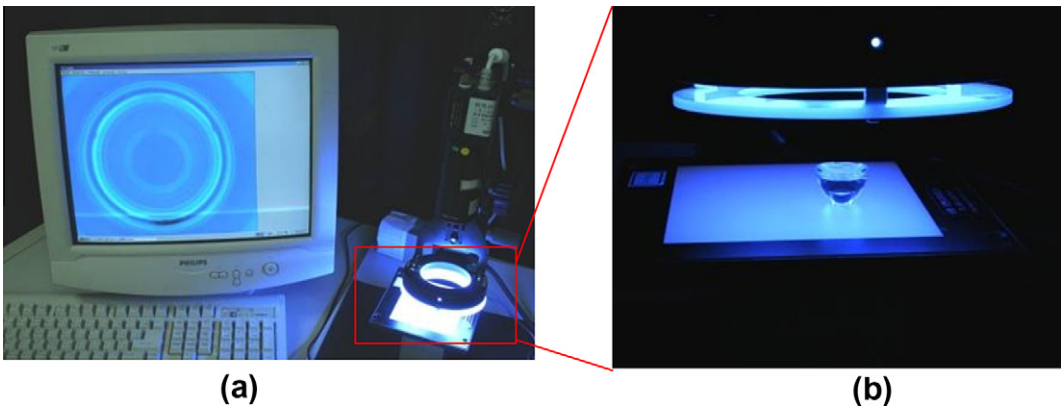

Fig. 8. Environmental configurations of scanning a testing LED lens sample: (a) hardware setup of experiments; (b) a testing LED lens sample is placed on XY table.

type I error α suggests the probability of producing false alarms, i.e. detecting normal regions as blemishes. Statistical type II error β implies the probability of producing missing alarms, which fail to alarm real blemishes. We divide the area of normal region detected as blemishes by the area of actual normal region to obtain type I error, and the area of undetected blemishes by the area of actual blemishes to obtain type II error. The correct classification rate (CR) is defined as:

$$CR = (N_{cc} + N_{dd})/N_{total} \times 100\%, \tag{22}$$

where N_{cc} is the pixel number of normal textures detected as normal areas, N_{dd} is the pixel number of blemishes detected as defective regions, and N_{total} is the total pixel number of a testing image.

Fig. 9 shows partial results of detecting visual blemishes by the Iterative method (Jain, Kasturi, & Schunck, 1995), the Otsu method (Otsu, 1979), Lin and Jiang method (Lin & Jiang, 2007), the proposed method, and the professional inspector, individually. The two spatial domain techniques, the Iterative and Otsu methods, make lots of erroneous judgments (false alarms) on visual blemish detection. The two frequency domain techniques, the Lin and Jiang approach and the proposed method, detect most of the visual blemishes and make less erroneous judgments. Therefore, the frequency domain approaches outperform the spatial domain techniques in the visual blemish detection of LED lenses.

Table 1 summarizes the detection results of our experiments. Two spatial domain approaches and two frequency domain techniques are evaluated against the results by professional inspectors. The average blemish detection rates $(1-\beta)$ of all testing samples by the four methods are, respectively, 98.86% (Iterative method), 99.84% (Otsu method), 86.23% (Lin and Jiang method), and 95.46% (proposed method). However, the two spatial domain methods have significantly higher false alarm rates (α), 28.96% (Iterative method) and 30.04% (Otsu method). On the contrary, the other two frequency domain approaches have rather lower false alarm rates, 0.01% (Lin and Jiang method) and 0.13% (proposed method). The proposed method has higher correct classifica-

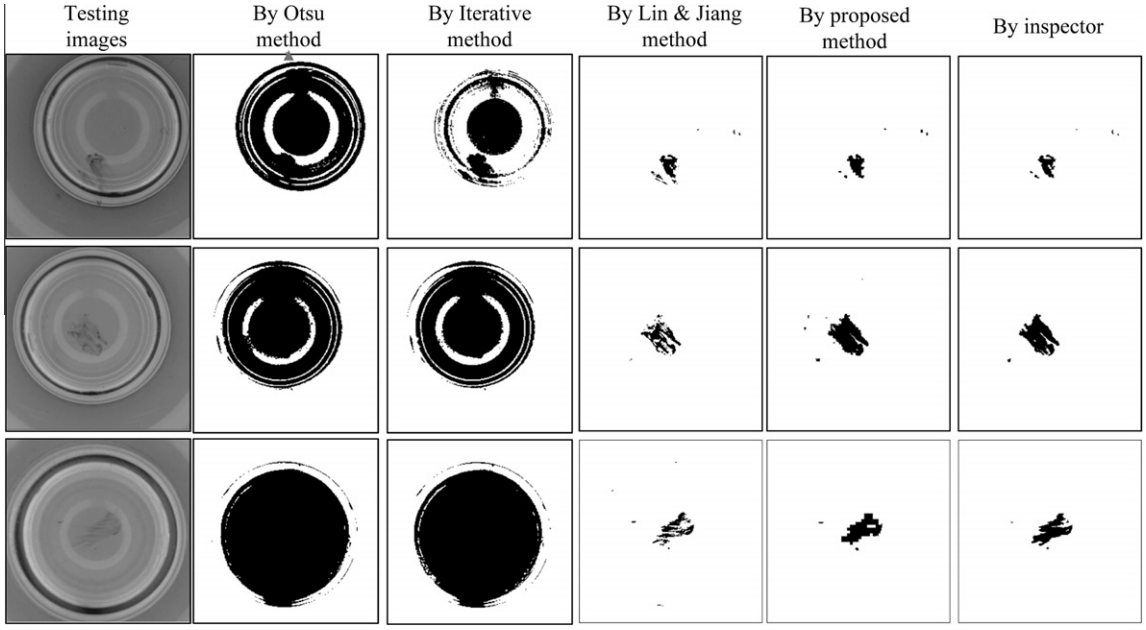

Fig. 9. Partial detection results of the Otsu, Iterative, Lin and Jiang, the proposed methods, and inspector.

Table 1
Summarized comparison table of visual blemish detection of LED lenses for four different methods.

	Spatial domain approaches		Frequency domain approaches	
	Otsu method	Iterative method	Lin and Jiang method	Proposed method
1-β (%)	99.84	98.86	86.23	95.46
α (%)	30.04	28.96	0.01	0.13
CR (%)	70.26	72.37	99.26	99.67
Time (s)	0.58	0.62	0.73	0.32

tion rates (CR) than do the other methods applied to blemish detection of LED lens images. More specifically, the proposed method has a higher detection rate than does the Lin and Jiang method but its false alarm rate is more than thirteen times higher than that of the latter method applied to LED lens images.

The average computation time for processing an image of 256×256 pixels is as follows: 0.58 s by the Otsu method, 0.62 s by the Iterative method, 0.73 s by the Lin and Jiang method, and 0.32 s by the proposed method. The average processing time of the proposed method is more than two times shorter than that of the Lin and Jiang method. The proposed method overcomes the difficulties of detecting visual blemishes on LED lens images with curved surfaces and excels in its ability of correctly discriminating visual blemishes from normal regions.

5. Concluding remarks

Machine vision systems improve productivity and quality management, and provide competitive advantages to industries that apply these systems. This research proposes an innovative vision system that applies BDCT, Hotelling's T-squared statistic, and grey clustering technique for the automatic detection of visual blemishes in curved surfaces of LED lenses. Real LED lenses are used as testing samples, and large-sample experiments are conducted in a real inspection environment to verify the performance of the proposed approach. Experimental results show that the proposed method achieves a high 95.46% probability of correctly discriminating visual blemishes from normal regions and a low 0.13% probability of erroneously detecting normal regions as blemishes on curved surfaces of LED lenses. Compared with other traditional methods, this approach has the advantages of higher detection rates, lower false alarm rates, and shorter average processing time. This method not only overcomes the difficulties of inspecting visual blemishes on curved surfaces but also relies on no template matching process.

The proposed method is based on feature extraction from BDCT-domain images for blemish detection. Since the computation of multivariate statistic is based on the mean vector and covariance matrix of training samples, the lighting changes may lead to the increase of variation in statistics and result in affecting the effect of blemish detection. It is recommended to re-compute the mean vector and covariance of the training samples when illumination is significantly changed. Future research may extend the proposed method to similar low-contrast blemish detection problems, such as abnormal inspection of medical images and tiny blemish detections of electronic and optical components. This research contributes a solution to a common surface blemish detection problem of optical lenses and offers a computer-aided visual blemish inspection system to meet the inspection and quality control request.

Acknowledgement

This work was partially supported by the National Science Council (NSC) of Taiwan, under Grant No. NSC 97-2221-E-324-020-MY3.

References

Ahmed, N., Natarajan, T., & Rao, K. R. (1974). Discrete cosine transform. *IEEE Transactions on Computer, 23*, 90–93.

Bazin, A. I., Cole, T., Kett, B., & Nixon, M. S. (2006). An automated system for contact lens inspection. *Lecture Notes in Computer Science, 4291*, 141–150.

Chan, C. H., & Pang, G. K. H. (2000). Fabric defect detection by Fourier analysis. *IEEE Transactions on Industry Applications, 36*, 1267–1276.

Chen, B., Latifi, S., & Kanai, J. (1999). Edge enhancement of remote sensing image data in the DCT domain. *Image and Vision Computing, 17*, 913–921.

Cho, C. S., Chung, B. M., & Park, M. J. (2005). Development of real-time vision-based fabric inspection system. *IEEE Transactions on Industrial Electronics, 52*, 1073–1079.

Deng, J. L. (1989). Introduction to grey system theory. *Journal of Grey System, 1*, 1–24.

Gonzalez, R. C., & Woods, R. E. (2008). *Digital image processing* (3rd ed.). New Jersey, USA: Prentice Hall.

Heng, Z. (2010). Analysis of infrared images based on grey system and neural network. *Kybernetes, 39*(8), 1366–1375.

Hu, Y. C., Chen, R. S., Hsu, Y. T., & Tzeng, G. H. (2002). Grey self-organizing feature maps. *Neurocomputing, 48*, 863–877.

Huang, K. Y. (2008). An auto-recognizing system for dice games using a modified unsupervised grey clustering algorithm. *Sensors, 8*, 1212–1221.

Jain, R., Kasturi, R., & Schunck, B. G. (1995). *Machine vision* (International Editions). New York, USA: McGraw Hill.

Kok, C. W. (1997). Fast algorithm for computing discrete cosine transform. *IEEE Transactions on Signal Processing, 45*, 757–760.

Latif-Amet, A., Ertüzün, A., & Ercil, A. (2000). An efficient method for texture defect detection: sub-band domain co-occurrence matrices. *Image and Vision Computing, 18*, 543–553.

Lin, H. D., & Ho, D. C. (2007). Detection of pinhole defects on chips and wafers using DCT enhancement in computer vision systems. *International Journal of Advanced Manufacturing Technology, 34*(5–6), 567–583.

Lin, H. D., & Jiang, J. D. (2007). Applying discrete cosine transform and grey relational analysis to surface defect detection of LED. *Journal of the Chinese Institute of Industrial Engineers, 24*(6), 458–467.

Lin, Y. H., & Lee, P. C. (2009). Effective evaluation model under the condition of insufficient and uncertain information. *Expert Systems with Applications, 36*, 5600–5604.

Lin, H. D., & Lin, W. T. (2009). Automated process adjustments of chip cutting operations using neural network and statistical approaches. *Expert Systems with Applications, 36*(3P1), 4338–4345.

Lin, H. D., Lin, G. C., Chung, C. Y., & Lin, W. T. (2008). Wavelet-based neural network and statistical approaches applied to automated visual inspection of LED chips. *Journal of Scientific & Industrial Research, 67*(6), 412–420.

Lin, C. H., Wu, C. H., & Huang, P. Z. (2009). Grey clustering analysis for incipient fault diagnosis in oil-immersed transformers. *Expert Systems with Applications, 36*, 1371–1379.

Madhuri, B., & Chandulal, J. (2010). Evaluating web sites using COPRAS GRA combined with grey clustering. *International Journal of Engineering Science and Technology, 2*(10), 5280–5294.

Martínez, S. S., Ortega, J. G., García, J. G., & García, A. S. (2009). A sensor planning system for automated headlamp lens inspection. *Expert Systems with Applications, 36*, 8768–8777.

Montgomery, D. C. (2009). *Statistical quality control: A modern introduction* (6th ed.). New York, NY, USA: John Wiley & Sons.

Montgomery, D. C., & Runger, G. C. (2007). *Applied statistics and probability for engineers* (4th ed.). New Jersey, USA: John Wiley & Sons.

Otsu, N. (1979). A threshold selection method from gray level histogram. *IEEE Transactions on Systems, Man and Cybernetics, 9*, 62–66.

Pan, F. (2002). Adaptive image compression using local pattern information. *Pattern Recognition Letters, 23*(14), 1837–1845.

Perng, D. B., Wang, W. C., & Chen, S. H. (2010). A novel quasi-contact lens auto-inspection system. *Journal of the Chinese Institute of Industrial Engineers, 27*(4), 260–269.

Rao, K. R., & Hwang, J. J. (1996). *Techniques and standards for image, video and audio coding*. New Jersey, USA: Prentice Hall PTR.

Rebsamen, M. J., Boucheix, M., & Fayol, M. (2010). Quality control in the optical industry: From a work analysis of lens inspection to a training programme, an experimental case study. *Applied Ergonomics, 41*, 150–160.

Tsai, D. M., & Hsiao, B. (2001). Automatic surface inspection using wavelet reconstruction. *Pattern Recognition, 34*, 1285–1305.

Tsai, H. C., Hsiao, S. W., & Hung, F. K. (2006). An image evaluation approach for parameter-based product form and color design. *Computer-Aided Design, 38*, 157–171.